The Hill analysis and co-ion–driven transporter kinetics

Juke S. Lolkema[1] and Dirk-Jan Slotboom[2]

[1]Department of Molecular Microbiology and [2]Department of Membrane Enzymology, Groningen Biomolecular Sciences and Biotechnology Institute, University of Groningen, 9747 AG Groningen, Netherlands

Interaction of multiple ligands with a protein or protein complex is a widespread phenomenon that allows for cooperativity. Here, we review the use of the Hill equation, which is commonly used to analyze binding or kinetic data, to analyze the kinetics of ion-coupled transporters and show how the mechanism of transport affects the Hill coefficient. Importantly, the Hill analysis of ion-coupled transporters can provide the exact number of transported co-ions, regardless of the extent of the cooperativity in ion binding.

The binding of oxygen to tetrameric hemoglobin is the textbook example for demonstrating interaction between multiple binding sites (cooperativity) on a biological unit and the use of the Hill equation (Hill, 1910). The Hill equation is derived from the analysis of the following binding equilibrium:

$$E + nL \overset{K_D}{\leftrightarrow} EL_n \qquad K_D = \frac{[E][L]^n}{[EL_n]}, \tag{1}$$

where E is a biological unit (hemoglobin, enzyme, receptor, transporter), L is a ligand, n is the stoichiometric coefficient of ligand L, and K_D is the (overall) dissociation constant. The saturation level of bound ligand is the same as the fraction of the biological unit in the substrate-bound state:

$$y = \frac{n[EL_n]}{n\varepsilon} = \frac{[EL_n]}{\varepsilon} \qquad \varepsilon = [E] + [EL_n]. \tag{2}$$

Substitution of the expression for the mass balance in the equilibrium constant yields the Hill equation,

$$y = \frac{[L]^n}{K_A^n + [L]^n} \qquad K_A = \sqrt[n]{K_D}, \tag{3}$$

where n is generally termed the Hill coefficient, and K_A indicates the ligand concentration that results in half of the maximal saturation level ($y = 0.5$). Parameters n and K_A may be determined from the slope and the ordinate intercept of a linearized form of the Hill equation,

$$\log\frac{y}{1-y} = n\log[L] - n\log K_A. \tag{4}$$

Binding equilibrium (Eq. 1) implies that the biological unit can bind n ligand molecules and, consequently, the Hill coefficient would correspond to the number of binding sites. As has been discussed extensively in the past, also by Hill himself, this conclusion is generally erroneous, because the derivation of equations (Eq. 3) is based on a physically unrealistic description of the binding events. Binding equilibrium (Eq. 1) describes an $(n + 1)$-molecular event in which n substrate molecules bind in a single step to the biological unit, which exists in two states only: the unloaded (E) and the fully occupied (EL_n) states. It does not take into account that partially occupied states (EL_1, EL_2, . . . EL_{n-1}) exist in real systems. In practice, the Hill coefficient obtained by fitting experimental binding data to the equation (Eq. 3 or 4) provides a measure for the cooperativity between the binding sites, taking a value of 1 in the absence of cooperativity and the number of binding sites in the extreme of infinite cooperativity.

Analyses of physically realistic models have been discussed extensively over the past century for biological systems consisting of identical subunits that each bind or catalyze the conversion of a ligand (Fig. 1, A and B) (Monod et al., 1965; Koshland et al., 1966; Perutz, 1989; Wyman and Gill, 1990). Well-studied examples include the binding of oxygen to tetrameric hemoglobin and carbamoyl group transfer between phosphate and aspartate by hexameric aspartate transcarbamoylase. These analyses have provided a more fundamental interpretation of the Hill coefficient as variable with ligand concentration (see, for instance, Wyman and Gill, 1990). The same basic concepts have been applied to the analysis of multimeric voltage- and ligand-gated channels that represent biological systems that are active in only one particular state of the complex (Fig. 1 C) (Weiss, 1997; Yifrach, 2004), for instance, a tetrameric ligand-gated channel that only opens after all four ligands have bound (Weiss, 1997). Ion-coupled transporters resemble

Correspondence to Dirk-Jan Slotboom: d.j.slotboom@rug.nl; or Juke S. Lolkema: j.s.lolkema@rug.nl

Abbreviation used in this paper: ITC, isothermal titration calorimetry.

The Rockefeller University Press
J. Gen. Physiol. Vol. 145 No. 6 565–574
www.jgp.org/cgi/doi/10.1085/jgp.201411332

these systems because they obligatorily bind several co-ions before the translocation event can take place. The co-ions bind to the same protein entity rather than to different subunits, but conceptually this makes no difference (Fig. 1 D). Nonetheless, physically realistic models are rarely used to analyze kinetic data of ion-coupled transporters, which is unfortunate, because a proper Hill analysis can be useful to obtain mechanistic understanding.

Here, we briefly review the Hill analysis of physically realistic models. We emphasize the importance of the measured output of the biological system by discriminating between a "binding" model and a "response" model, which have different information content. Ion-coupled transporters represent a clear example of the response model, and we subsequently describe the Hill analysis of transporter kinetics. As an example, we show how the analysis can provide the exact number of transported co-ions, regardless of the extent of cooperativity in ion binding. Finally, we use the large amount of available data on the sodium-coupled aspartate transporter Glt_{Ph} to exemplify the usefulness of the Hill analysis.

The saturation curves in binding and response models

In realistic models, the ligand molecules bind sequentially to the N binding sites on the biological unit, thereby generating intermediate bound states as demonstrated in the example with $N = 2$ in Fig. 2. As a consequence, the mass balance changes to

$$\varepsilon = [E] + [E_{(a)}L] + [E_{(b)}L] + [ELL], \tag{5}$$

where subscripts (a) and (b) indicate the two binding sites on E. It follows that the saturation level depends on what exactly is measured.

The binding model applies when the binding of each substrate molecule evokes the same measurable output (Fig. 2 A) and the saturation curve is defined by

$$y_B = \frac{[E_{(a)}L] + [E_{(b)}L] + 2[ELL]}{2\varepsilon}. \tag{6}$$

Examples include the binding of a radiolabeled ligand to a receptor, the binding of oxygen to hemoglobin where each bound oxygen molecule gives rise to the same spectral change, or enzyme catalysis in multimeric complexes where each subunit contains a catalytic site.

The saturation curve of the response model is different, because the experimentally determined output is not proportional to the amount of bound ligand, but rather to the concentration of one particular state. Often, the productive state is the fully occupied state ELL (Fig. 2 B), and the corresponding saturation curve is defined by

$$y_R = \frac{[ELL]}{\varepsilon}. \tag{7}$$

Examples of such biological systems include ligand-gated channels that open only when all sites are occupied, receptors that signal in the fully occupied state, and also ion-coupled transporters that translocate when all co-ions have bound (Fig. 1, C and D). The same biological system may be analyzed by both models depending on the experimental setup. In one experiment, radiolabeled ligand bound to a channel may be measured at varying free ligand, and in a second experiment, the current through the same channel may be monitored. The two approaches yield different saturation behaviors.

The relation between the saturation level y_B and the concentration of the free ligand in the binding model for a system with two identical binding sites is

$$y_B = \frac{\alpha K_D[L] + [L]^2}{\alpha K_D^2 + 2\alpha K_D[L] + [L]^2} \qquad K_A = K_D\sqrt{\alpha}. \tag{8}$$

Interaction parameter α gives the change in affinity of one site when the other site is already occupied ($K_D^* = \alpha K_D$; see Fig. 2). α takes a value of 1 in the absence of cooperativity and a value of <1 for positive cooperativity, and thus is inversely related to cooperativity. For

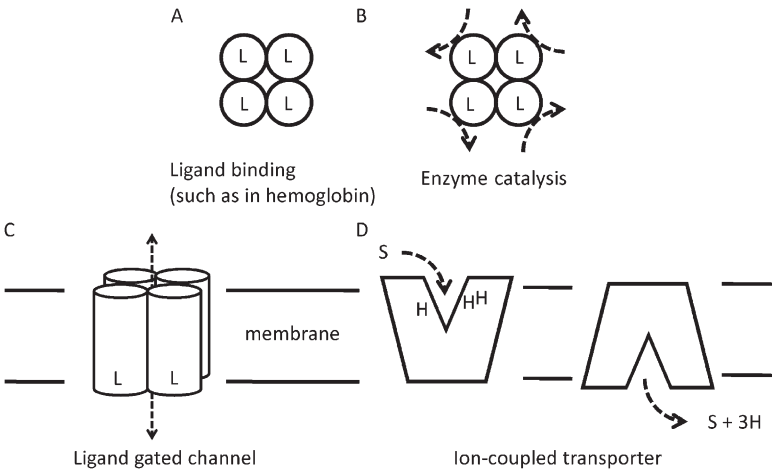

Figure 1. Models for multiple ligand binding to biological systems. (A) Tetrameric complex. Each subunit binds ligand L. (B) Tetrameric enzyme. Each subunit catalyzes the conversion (dashed arrows) of ligand L. (C) Tetrameric ligand-gated channel. The channel opens when all subunits have bound ligand L. The dashed arrow indicates the ion flow through the open channel. (D) Ion-coupled transporter. Substrate S is translocated in symport with three co-ions H.

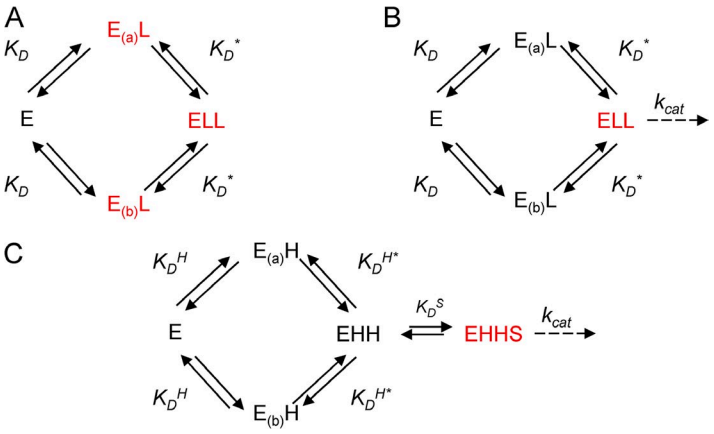

Figure 2. Mechanistic models of ligand binding. (A and B) The binding and response models. Binding schemes of ligand L to a biological unit E containing two ligand-binding sites *a* and *b* ($N = 2$). The dissociation constant K_D refers to the binding to either of the two free sites, whereas K_D* refers to binding to one site with the other site occupied. Red states contribute to the measured output. (C) The ordered-binding transporter mechanism. Substrate *S* and two co-ions *H* bind to a transporter E ($N = 2$). K_D^{H*} equals αK_D^H in which α is the interaction parameter.

a similar system, the saturation level y_R in the response model, takes the form

$$y_R = \frac{[L]^2}{\alpha K_D^2 + 2\alpha K_D[L] + [L]^2} \qquad K_A = K_D\left(\alpha + \sqrt{\alpha^2 + \alpha}\right). \quad (9)$$

See supplemental text 1 for the derivations. Relations (Eqs. 8 and 9) differ by the term $\alpha K_D[L]$ in the numerator of y_B, such that $y_B > y_R$ at every ligand concentration. The different saturation behavior is immediately evident for the case where there is no interaction between the binding sites, i.e., $\alpha = 1$ (no cooperativity). Then,

$$y_B = \frac{[L]}{K_D + [L]} \quad (10)$$

$$y_R = \frac{[L]}{[L] + K_D}\frac{[L]}{[L] + K_D} \quad (11)$$

$$\alpha = 1$$

The binding model (Eq. 10) behaves like binding to a single site following a simple hyperbolic saturation curve. In contrast, the response model produces a sigmoidal saturation curve (Eq. 11), even in the absence of interaction. It is the product of the occupancy of the two independent binding sites, representing the probability of one site being occupied when the other is occupied as well, i.e., the *ELL* state.

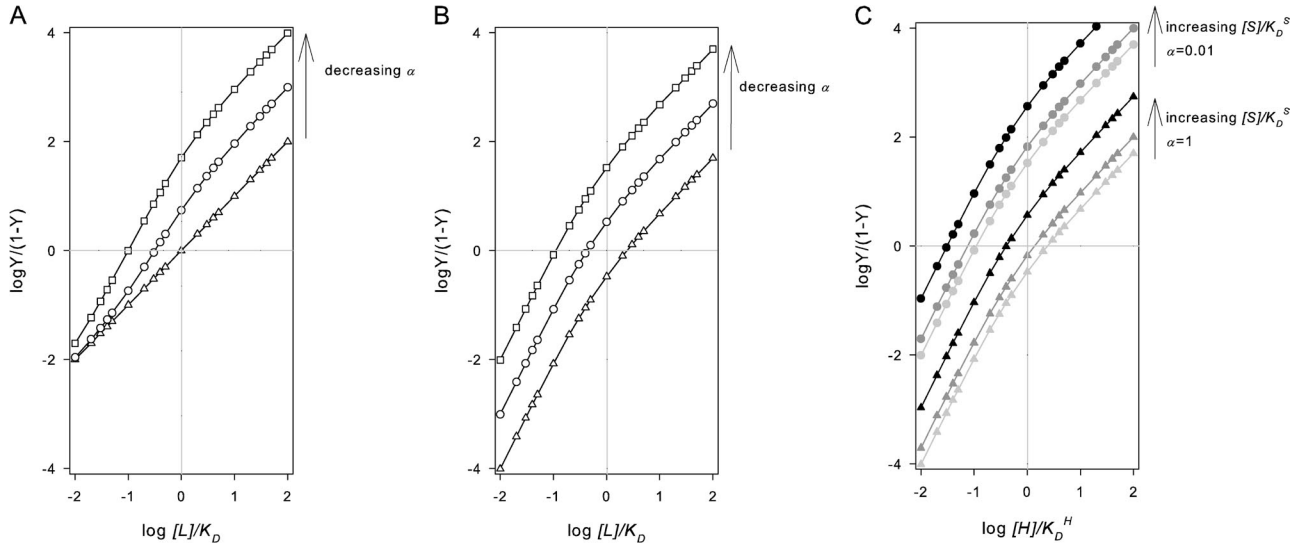

Figure 3. Hill analysis of the saturation curve in the binding model (A), the response model (B), and an ion-coupled transporter catalyzing an ordered-binding mechanism (C). Saturation levels were calculated using Eqs. 8 and 9 for A and B, respectively, for three values of the interaction parameter α: 1 (△), 0.1 (○), and 0.01 (□). For plot C, saturation levels were calculated using Eq. 21 for two values of the interaction parameter α: 1 (triangles) and 0.01 (circles), and three values of the substrate concentration relative to K_D^S: 1 (light gray), 10 (dark gray), and 100 (black). The Hill analyses of the saturation curves are presented in supplemental text 3. In all cases, half saturation is observed at the x-axis intercept.

Hill analysis of the binding and response models

Even though the saturation curves for the binding and response models (Eqs. 8 and 9) do not take the form of the Hill equation (Eq. 3), the experimental data can be analyzed by a double logarithmic plot similar to Eq. 4:

$$log\frac{y_{B/R}}{1-y_{B/R}} = f\left(log[L]\right). \quad (12)$$

In contrast to the linear relation described by Eq. 4, the slope of the curve obtained from the Hill analyses of realistic models is a variable with the ligand concentration, and the Hill coefficient n is redefined as the slope of the curve at $[L] = K_A$, where y is half the maximal saturation level (Kuriyan et al., 2012). In Fig. 3 (A and B), the Hill analyses for the binding and response models are presented for three different cases: no interaction between the binding sites (independent binding, $\alpha = 1$), strong interaction ($\alpha = 0.01$), and an intermediate level of interaction ($\alpha = 0.1$).

For all values of α, the binding model yields linear relations both at very low ($[L] << K_D$) and very high ($[L] >> K_D$) ligand concentrations, with slopes equal to 1 (Fig. 3 A and supplemental text 3). In the absence of interaction ($\alpha = 1$), the two lines are continuous in line with Eq. 10. With interacting sites ($\alpha < 1$), the two linear parts are discontinuous, and the slope of the curve is maximal at $[L] = K_A$. The Hill coefficient defined as the slope at $[L] = K_A$ depends on the interaction between the sites and takes a value between 1 and N, the number of binding sites.

The Hill analysis of the response model results in a curve with a different shape (Fig. 3 B). Again, there are linear parts at the high and low extremes of the ligand concentration for every value of α, but in this case with different slopes. At the high concentration limit, the slope approaches a value of 1, but at the low limit it approaches a value of N (see supplemental text 3), which is the maximal slope of the curve. With increasing interaction between the sites, the entire curve shifts up the y axis, but the shape remains identical. Consequently, regardless of the interaction between the sites, the Hill analysis of the response model always contains the information on the number of binding sites in the slope of the linear part at the lower concentration limit. The Hill coefficient defined as the slope at the x-axis intercept is always smaller than the maximal slope of the curve. In the limit of very high cooperativity, it approaches the number of binding sites N. In the absence of interaction between the binding sites, the slope is larger than 1, in line with Eq. 11.

In contrast to the Hill coefficient, the interaction parameter α in the mechanistic binding and response models is a true measure of the interaction between the sites. Parameter α measures the change in affinity of one site upon binding to the other site ($K_D{*} = \alpha K_D$). The relation between the Hill coefficient and the mechanistic interaction parameter α is shown in Fig. 4 A for the binding and response models analyzed above. It requires an increase in the affinity of a factor of ~10 (α = 0.1) for the Hill coefficient to reach a value that is halfway between 1 and the number of binding sites (n = 1.5). It follows that the interaction has to be extremely strong for the Hill coefficient to approach the number of binding sites.

Ion-coupled transporters

Ion-coupled secondary transporters allow for the accumulation of a substrate S inside the cell by catalyzing the following transport reaction

$$S_{out} + nH_{out} \rightarrow S_{in} + nH_{in}, \quad (13)$$

in which H is the co-ion, usually a proton or Na^+ ion, and n equals the number of symported co-ions. Free energy is transduced from the co-ion gradient, the proton motive force or sodium ion motive force, to the substrate gradient. Mechanistically, secondary transporters

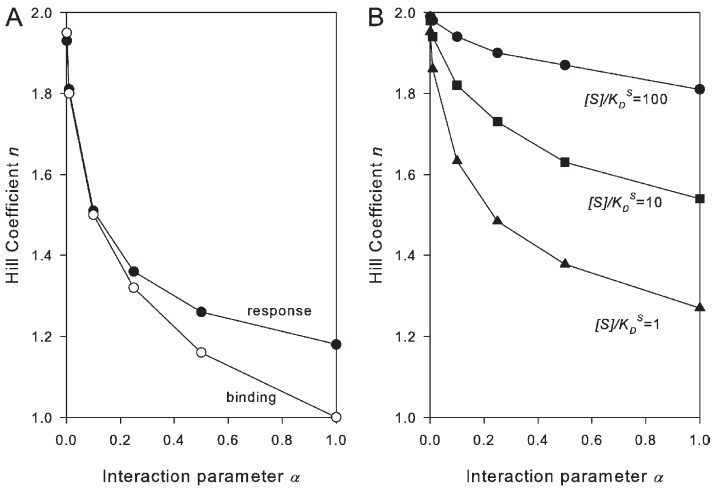

Figure 4. Relation between the Hill coefficient n and the mechanistic interaction parameter α. The Hill coefficient n was determined graphically at different values of interaction parameter α in the binding model (A; ○) and the response model (A; ●) and for the ordered-binding transporter mechanism with the substrate concentration poised at K_D^S (B; ▲), $10{*}K_D^S$ (B; ■), and $100{*}K_D^S$ (B; ●). Data points close to the x-axis intercept of the Hill plots (Fig. 3) were fitted to a straight line by least-square fits. The slope of the best fit was taken as the Hill coefficient.

couple the flux of the substrate to the flux of the co-ions by allowing the actual translocation step only when the transporter protein has bound the full complement of transported species (the productive state),

$$E + S_{out} + nH_{out} \overset{K_D}{\leftrightarrow} E:S:H_n \overset{k_{cat}}{\rightarrow} \qquad K_D = \frac{[E][S][H]^n}{[ESH_n]}. \quad (14)$$

The binding equilibrium in Eq. 14 resembles the one in Eq. 1 where the co-ions are concerned, but an additional ligand, the substrate, is bound as well. The Hill equation may be derived using an analogous approach as above for binding equilibrium (Eq. 1).

The rate is proportional to the concentration of state $E:S:H_n$ and maximal (V_{max}) when all enzyme ε is in the productive state:

$$v = k_{cat}[E:S:H_n] \qquad V_{max} = k_{cat}\varepsilon \qquad \varepsilon = [E] + [E:S:H_n]. \quad (15)$$

Substitution of the mass balance in the expression for the overall equilibrium constant K_D in Eq. 14, and assuming rapid equilibrium of the binding steps, yields Eq. 16 for the saturation level of the rate:

$$y = \frac{v}{V_{max}} = \frac{[E:S:H_n]}{\varepsilon} = \frac{[S][H]^n}{K_D + [S][H]^n}. \quad (16)$$

Because two different molecules (S and H) are transported by the protein, the analysis of y depends on the experimental design. In one type of experiment, the saturation level is measured at constant substrate concentration and varying co-ion concentration for which reorganization of the terms in Eq. 16 results in the Hill equation,

$$y = \frac{[H]^n}{K_A^n + [H]^n} \qquad K_A = \sqrt[n]{\frac{K_D}{[S]}}. \quad (16a)$$

The concentration of H yielding half the maximal rate (K_A) depends on the substrate concentration. The Hill coefficient n may be derived using Eq. 4.

Alternatively, the saturation level is measured at constant co-ion concentration and varying substrate concentration, which yields the equivalent relation,

$$y = \frac{[S]}{K_D^S(app) + [S]} \qquad K_D^S(app) = \frac{K_D}{[H]^n}. \quad (16b)$$

The apparent affinity constant for the substrate ($K_D{}^S$ (app)) depends on the co-ion concentration, and Hill coefficient n may be determined from the slope of a double logarithmic plot of the apparent affinity constant and the co-ion concentration,

$$\log K_D^S(app) = \log K_D - n\log[H] \quad (17)$$

(see also Boudker et al., 2007; Verdon et al., 2014).

This type of analysis may lead to erroneous interpretations of n because any mechanistic detail is ignored. Similarly, as discussed above, the value of n does not report the number of co-ions.

Mechanistic transporter models

Ion-coupled transporters are of the response model type, because only the state with all co-ions bound is translocation competent. The binding of co-ions as well as the substrate not only allows for interaction between the co-ion–binding sites but also for interaction between co-ion– and substrate-binding sites. Two extreme cases are the "random-binding" mechanism that assumes no interaction between co-ion– and substrate-binding sites and the "ordered-binding" mechanism that assumes that all co-ions bind before the substrate can bind. Note that "random" and "ordered" are used here to indicate the interaction between substrate and co-ions, not between co-ions.

In the random-binding mechanism, the co-ions bind according to the scheme in Fig. 2 B (for $N = 2$), where the substrate binds with the same affinity to all states of the transporter regardless of the number of co-ions bound. The saturation level of the rate is the product of the saturation levels of co-ion binding in the response model $y_R{}^H$ (Eq. 9) and substrate binding $y_R{}^S$ (supplemental text 1, section 1.1):

$$y_R = \frac{v}{V_{max}} = y_R^H y_R^S. \quad (18)$$

It follows for the rate measured at varying co-ion concentration at constant substrate concentration,

$$v = V_{max}(app)\, y_R^H \qquad V_{max}(app) = \frac{[S]}{K_D^S + [S]} V_{max}. \quad (18a)$$

Similarly, for the rate of substrate-dependent measurements at constant co-ion concentration,

$$v = V_{max}(app)\frac{[S]}{K_D^S + [S]} \qquad V_{max}(app) = y_R^H V_{max}. \quad (18b)$$

In the random-binding mechanism, the ligand for which the concentration is kept constant in the experiments (either the co-ion or the substrate) affects the maximal rate, but not the affinity for the other ligand.

In the ordered-binding mechanism, the substrate has affinity only for the fully co-ion–loaded state, resulting in the scheme depicted in Fig. 2 C ($N = 2$). It can be shown for the saturation level of the rate (see supplemental text 2) that

$$y_R = \frac{y_R^H [S]}{K_D^S + y_R^H [S]}, \quad (19)$$

and it follows for co-ion–dependent rate measurements at constant substrate,

$$v = V_{max}(app)\frac{y_R^H}{\frac{K_D^S}{K_D^S+[S]}+\frac{[S]}{K_D^S+[S]}y_R^H} \qquad V_{max}(app) = \frac{[S]}{K_D^S+[S]}V_{max}. \tag{19a}$$

Unlike for the random-binding mechanism (Eq. 18a), the apparent affinity of the co-ions is dependent on the fixed substrate concentration for the ordered-binding mechanism. See supplemental text 2, section 2.2.2, for the relation between K_A, the concentration of H that results in half the maximal rate, and the concentration of S.

In case of substrate-dependent rate measurements at constant co-ion concentration, Eq. 19b applies:

$$v = V_{max}\frac{[S]}{K_D^S(app)+[S]} \qquad K_D^S(app) = \frac{K_D^S}{y_R^H}. \tag{19b}$$

The substrate "pulls" the transporter in the productive state, but this requires a higher concentration when the co-ion concentration is low than when it is high; i.e., the apparent affinity for the substrate increases with higher co-ion concentration. Eventually, all transporter molecules will be pulled in the productive state, making the maximal rate independent of the co-ion concentration.

Measurement of $K_D{}^S(app)$ and $V_{max}(app)$ at several different co-ion concentrations provides a means of discriminating between the two extreme mechanisms of random binding and ordered binding. In the random-binding mechanism, the co-ion concentration affects the maximal rate, whereas the affinity for the substrate is not affected, and in the ordered-binding mechanism, the affinity for the substrate depends on the co-ion concentration, whereas the maximal rate is independent. A more detailed account of substrate-dependent transport kinetics is given in supplemental text 4.

Hill analysis of mechanistic transporter models

The Hill analysis of the transport rate measured at varying co-ion concentrations and constant substrate implies

$$\log\frac{y_R}{1-y_R} = \log\frac{v}{V_{max}-v} = f(\log[H]). \tag{20}$$

In the random-binding mechanism, the saturation behavior for the co-ions (Eq. 18a) is identical to the response model (Eq. 9), and consequently the graphical analysis of Eq. 20 is identical to Fig. 3 B.

In the ordered-binding mechanism, substitution of the expression for $y_R{}^H$ in Eq. 19a yields for a transporter with two binding sites ($N = 2$; see supplemental text 2, section 2.2),

$$v = V_{max}(app)\frac{[H]^2}{\alpha(app)K_D^{H\,2}+2\alpha(app)K_D^H[H]+[H]^2} \tag{21}$$
$$\alpha(app) = \alpha\frac{K_D^S}{K_D^S+[S]}.$$

Importantly, the interaction parameter α is replaced by an apparent interaction parameter $\alpha(app)$ that depends on the substrate concentration $[S]$. At constant substrate concentration, Eq. 21 is of the same form as the saturation level function of the response model (Eq. 9). In the Hill analysis, the shape of the curves is identical as that observed for the response model above, but the curves shift up along the y axis by a value of $\log(1 + [S]/K_D)$ (Fig. 3 C, for two values of α, and supplemental text 3, section 3.3). The upshift moves the x-axis intercept into the low substrate concentration domain and, consequently, higher values for the Hill coefficient are obtained with increasing concentrations of the substrate S used in the experiments (Fig. 5, A and B). The maximum value for n still equals the number of binding sites N. Importantly, the concentration of S is an experimental variable, and therefore the value of n can be controlled experimentally (see below).

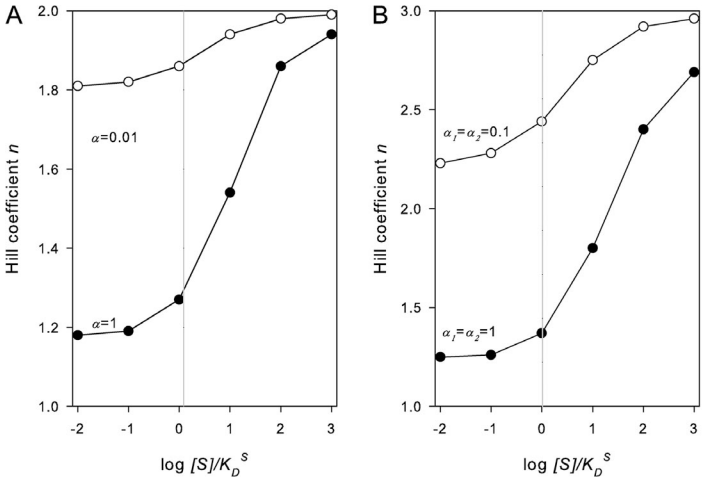

Figure 5. Dependence of the Hill coefficient on the substrate concentration in the ordered-binding mechanism of a transporter with two co-ion–binding sites ($N = 2$) and $\alpha = 1$ (●) and $\alpha = 0.01$ (○; A) and with three co-ion–binding sites ($N = 3$) and $\alpha_1 = \alpha_2 = 1$ (●) and $\alpha_1 = \alpha_2 = 0.1$ (○; B). The Hill coefficients were determined as described in the legend to Fig. 4.

Relation between the Hill coefficient and cooperativity in the ordered-binding transporter model

In the ordered-binding transporter model, the apparent interaction between the co-ions increases with increasing substrate concentration and, consistently, the simulations in Fig. 4 B show an increase in the Hill coefficient with increasing [*S*] at every value of α. The Hill coefficient is most sensitive to the substrate concentration in the absence of interaction between the sites (Fig. 4 B). If there is strong interaction between the co-ions ($\alpha = 0.01$), the dependency is much smaller and the value of n much closer to N over the entire range of substrate concentrations (Fig. 5, A and B, for $n = 2$ and $n = 3$, respectively).

The ordered-binding mechanism of the co-ion–coupled transporter resembles the behavior of ligand-activated receptors described by Weiss (1997). He noted that a transition of a receptor in the fully bound state to a second fully bound state had the same effect as an increased interaction between the ligand-binding sites. The example used was a receptor with multiple ligand-binding sites that could convert from an inactive state to an activated state only if all ligands were bound. The more the activated state was favored in the equilibrium between the two states, the more the Hill coefficient approached the number of binding sites. Similarly, in the ordered-binding mechanism of the co-ion–coupled transporter, the productive state EH_n is selectively "pulled out" of the co-ion–binding scheme by the substrate to yield state EH_nS. Importantly, in the case of transporters, the (apparent) equilibrium between the two states is experimentally accessible by setting the substrate concentration. At infinite high substrate concentration, the number of co-ions is reported by the Hill coefficient independent of the interaction between the co-ion–binding sites.

Practical consideration: Data analysis

Experimentally, the Hill coefficient is determined by measuring transport rates in a narrow range of co-ion concentrations around the concentration that yields half the maximal rate (i.e., K_A). The data are then plotted according to Eq. 20 and fitted to a straight line, the slope of which is taken as the Hill coefficient. Importantly, a fair estimation of the maximal rate is needed for this analysis. Alternatively, the experimental data may be fitted directly to the Hill equation (Eq. 3) using a nonlinear fitting procedure, which takes both the Hill coefficient and the maximal rate as parameters. Formally, this procedure is incorrect because the equation does not describe the response model, but the numeric results are practically the same between the two methods (see supplemental text 5).

To determine the number of cotransported ions in secondary transporters, there are three options. The first option applies when transport follows an ordered-binding mechanism. The Hill coefficients are determined at a range of substrate concentrations (Fig. 5). The number of co-ions follows from the value that the Hill coefficient approaches at high substrate concentration (see below for example). The Hill coefficient at low substrate concentrations reports on the interaction between the co-ion–binding sites. The second option applies regardless of whether the transporter catalyzes a random-binding or ordered-binding mechanism. The number of sites may be directly obtained from the saturation level curve at the lower co-ion concentration limit. In this case, only the first term is significant in the denominator of Eq. 9 and in the equivalent equations in supplemental text 1, Table 1.4. This limit corresponds to the condition where bound states of the biological unit are negligible, and the saturation level is

$$y_R^H \sim [H]^N \qquad y_R^H << 1. \tag{22}$$

When experimental conditions allow, Eq. 22 provides a direct estimate of the number of binding sites (see, for instance, Lolkema et al., 1994). This approach resembles the limiting slope analysis of voltage-gated ion channels (Sigworth, 1994; Zagotta et al., 1994; Bezanilla, 2000).

Finally, true mechanistic information may be obtained by fitting the data directly to the saturation curves y_R. Unfortunately, there is no continuous function in N, and the data subsequently has to be fitted to the equations for $n = 1$, $n = 2$, . . . (see supplemental texts 1 and 2, sections 1.4 and 2.4). Once the number of co-ions is determined by the best-fitting equation, the interaction parameters α_i are obtained from the fitted parameters. Although this procedure yields the most detailed information, it requires highly accurate data to be successful.

Example: The Na^+-coupled aspartate transporter Glt_{Ph}

The aspartate transporter Glt_{Ph} of the archaeon *Pyrococcus horikoshii* was among the first ion-coupled transporters for which a high resolution crystal structure was obtained (Yernool et al., 2004). Glt_{Ph} is a member of the DAACS family of transporters that contains members from all domains of life, ranging from transporters for glutamate and neutral amino acid uptake in bacteria to excitatory neurotransmitter transporters in the central nervous system (Slotboom et al., 1999; Focke et al., 2013). The crystal structure of Glt_{Ph} prompted many functional studies of the transporter to relate structure to mechanism (Boudker et al., 2007; Ryan and Mindell, 2007; Reyes et al., 2009, 2013; Ryan et al., 2009; Groeneveld and Slotboom, 2010; Akyuz et al., 2013, 2015; Erkens et al., 2013; Ewers et al., 2013; Hänelt et al., 2013; Jensen et al., 2013; Mulligan and Mindell, 2013; Verdon et al., 2014; Focke et al., 2015; Machtens et al., 2015). For the discussion here, it is relevant that rates of aspartate transport as a function of the co-ion concentration have been

measured at fixed aspartate concentrations, and conversely, that apparent affinity constants for aspartate have been measured at fixed co-ion concentrations (Boudker et al., 2007; Reyes et al., 2013; Verdon et al., 2014).

Analysis of transport data. Ryan et al. (2009) reported the rate of transport catalyzed by Glt_{Ph} reconstituted in proteoliposomes as a function of the Na^+ concentration at two fixed aspartate concentrations using transport assays with radiolabeled aspartate. At a fixed concentration of 0.1 µM aspartate, a sigmoidal relation was obtained that fitted to the Hill equation (Eq. 3) with an apparent affinity K_A of 3.9 mM Na^+ and a Hill coefficient n of 2.4. At a 10-fold higher aspartate concentration, the curve as a whole shifted to lower Na^+ concentrations resulting in a higher apparent affinity K_A of 2.0 mM and a slightly higher Hill coefficient of 2.6. The change in apparent affinity indicates that the mechanism of transport by Glt_{Ph} is not of the random-binding type (Eq. 18a). The random-binding and ordered-binding mechanisms described above are extreme cases. The data suggests that Glt_{Ph} has a significant ordered-binding component following Eq. 19a. The ordered-binding mechanism for Glt_{Ph} is in agreement with experiments showing a much lower affinity of the protein for aspartate in the absence than in the presence of Na^+ (Boudker et al., 2007; Jensen et al., 2013).

In the ordered-binding mechanism, the Hill coefficient increases with increasing substrate concentration to reach the number of co-ions transported (Fig. 5). In the experiments of Ryan et al. (2009), the Hill coefficient is relatively insensitive to the 10-fold increase in aspartate concentration (it raises from 2.4 to 2.6) and is close to the number of three transported Na^+ ions determined independently by direct measurement of the flux ratio between aspartate and Na^+ using ^{14}C-labeled aspartate and $^{22}Na^+$ (Groeneveld and Slotboom, 2010). The two fixed aspartate concentrations of 0.1 and 1 µM roughly correspond with values of 1 and 10 for the ratio $[S]/K_D^S$ (K_M^{asp} = 0.12 µM at 100 mM Na^+; Ryan et al., 2009). The relatively small increase in the Hill coefficient between these two values suggests significant cooperativity between the Na^+-binding sites on Glt_{Ph} (Fig. 5 B). It must be emphasized that the apparent affinities and Hill coefficients should be determined over a much larger range of aspartate concentrations to confirm these conclusions.

Analysis of aspartate affinity constants. Apparent affinities of Glt_{Ph} for aspartate at different fixed sodium ion concentrations have been determined by isothermal titration calorimetry (ITC) or fluorescence signal titrations for the wild-type protein and binding-site mutants (Boudker et al., 2007; Reyes et al., 2013; Verdon et al., 2014). The data showed a strong dependence of the K_D values for aspartate on the Na^+ ion concentration and was analyzed by Eq. 17, which indicates a linear relation in a double logarithmic plot of the apparent affinity constant and the fixed co-ion concentration with a slope identical to the number of sodium ions. The experimental data in some cases fitted well to a linear relation but in other cases deviated strongly (Reyes et al., 2013). Slopes of the fitted lines in different experiments varied from 0.7 to 2.9.

As discussed above, Eq. 17 ignores any mechanistic detail by not taking into account partially Na^+-bound states. Analysis of a more realistic mechanistic model is presented in supplemental text 4, and a graphical representation is shown in Fig. 6. Only in the low sodium ion concentration range is the relation linear with a slope that reports the number of co-ions. With increasing co-ion concentration, the slope decreases to become zero and the affinity constant extrapolates to the true K_D for aspartate when the protein is saturated with sodium ions. The nonlinearity is well visible in the experimental data, and a slope of <1 has been reported (e.g., Verdon et al., 2014). Consequently, the range of co-ion concentrations used in the experiments must be large enough to cover the full shape of the curve. If not, the slope may be any number between zero and the number of co-ions.

It must be noted that the analysis of binding data obtained by ITC or fluorescence techniques is less straightforward than the analysis of transport data. In contrast to measurements of transport rates, in which the response is proportional to the fully Na^+-bound state, with ITC or fluorescence measurements, it is not known "a priori" to which Na^+-bound state aspartate binds; i.e., the results do not discriminate between a binding and a response model for co-ion binding. In the reported

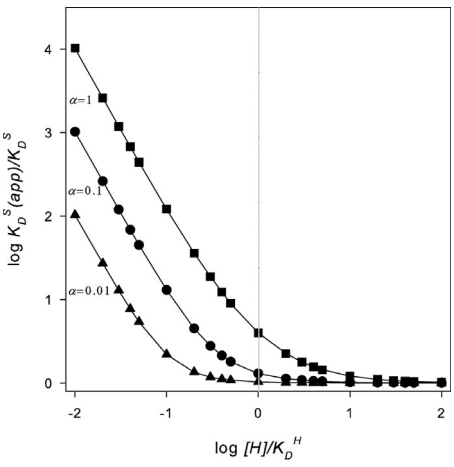

Figure 6. Analysis of the apparent affinity for the substrate in the ordered-binding mechanism. The plot shows numerical simulations of Eq. 4.13 in supplemental text 4 for three values of the interaction parameter α: 1 (■), 0.1 (●), and 0.01 (▲). The function was rewritten to $K_D^S(app)/K_D^S = \alpha + 2\alpha x + x^2/x^2$, in which x is the co-ion concentration relative to the affinity constant ($x = [H]/K_D^H$).

binding experiments for Glt_{Ph}, only the binding of aspartate and not the binding of Na^+ was detected, as binding of Na^+ alone did not generate a measurable fluorescence change nor a detectable heat release. The strong dependence of the affinity constant for aspartate on the Na^+ concentration indicates an ordered-binding type of mechanism where aspartate preferentially binds to Na^+-bound states.

Conclusion

In mechanistic models for binding of multiple ligands to a biological unit, the saturation behavior depends on the experimental readout. In the binding model, the Hill analysis does not provide information on the number of binding sites *N*. In contrast, the Hill analysis of the response model does contain this information, in which case the slope of the curve in the lower concentration range corresponds to the number of binding sites. In neither model does the Hill coefficient—defined as the slope of the curve at half-maximal saturation—report this number. In the binding model, the Hill coefficient varies between a value of 1 in the absence of interaction and a value of *N* in case of extremely strong interaction. In the response model, it varies between a number larger than 1 and *N*. In both models, the derived Hill coefficient is a measure of the cooperativity and sets a lowest possible number of sites.

Ion-coupled transporters are of the response model type, and the saturation behavior of the rate with the co-ion in the lower concentration limit contains the information on the number of cotransported ions. Additionally, in the case of an ordered-binding mechanism, in which the co-ions bind before the transported substrate, the Hill coefficient of co-ion binding is a function of the substrate concentration. The apparent interaction between the co-ion sites increases with the substrate concentration and, consequently, the Hill coefficient extrapolates to the number of co-ions. Measurements of the Hill coefficient over the entire range of substrate concentrations provide information on both the extent of interaction between the sites and the number of sites.

Online supplemental material

Five supplemental texts accompany this review: (1) derivation of the equations for the binding and response models; (2) derivation of the equations for the ordered-binding transporter mechanism; (3) derivation of the equations for the Hill analysis of the saturation level functions; (4) derivation of the equations for substrate-dependent kinetics of mechanistic transporter models; (5) data analysis by curve fitting. The online supplemental material is available at http://www.jgp.org/cgi/content/full/jgp.201411332/DC1.

This work was funded by the Netherlands Organization for Scientific Research (NWO; NWO ECHO grant 711.011.001 and NWO Vici grant 865.11.001) and the European Research Council (ERC; ERC Starting Grant 282083).

The authors declare no competing financial interests.

Merritt C. Maduke served as editor.

Submitted: 21 November 2014
Accepted: 7 April 2015

REFERENCES

Akyuz, N., R.B. Altman, S.C. Blanchard, and O. Boudker. 2013. Transport dynamics in a glutamate transporter homologue. *Nature.* 502:114–118. http://dx.doi.org/10.1038/nature12265

Akyuz, N., E.R. Georgieva, Z. Zhou, S. Stolzenberg, M.A. Cuendet, G. Khelashvili, R.B. Altman, D.S. Terry, J.H. Freed, H. Weinstein, et al. 2015. Transport domain unlocking sets the uptake rate of an aspartate transporter. *Nature.* 518:68–73. http://dx.doi.org/10.1038/nature14158

Bezanilla, F. 2000. The voltage sensor in voltage-dependent ion channels. *Physiol. Rev.* 80:555–592.

Boudker, O., R.M. Ryan, D. Yernool, K. Shimamoto, and E. Gouaux. 2007. Coupling substrate and ion binding to extracellular gate of a sodium-dependent aspartate transporter. *Nature.* 445:387–393. http://dx.doi.org/10.1038/nature05455

Erkens, G.B., I. Hänelt, J.M.H. Goudsmits, D.J. Slotboom, and A.M. van Oijen. 2013. Unsynchronised subunit motion in single trimeric sodium-coupled aspartate transporters. *Nature.* 502:119–123. http://dx.doi.org/10.1038/nature12538

Ewers, D., T. Becher, J.-P. Machtens, I. Weyand, and C. Fahlke. 2013. Induced fit substrate binding to an archeal glutamate transporter homologue. *Proc. Natl. Acad. Sci. USA.* 110:12486–12491. http://dx.doi.org/10.1073/pnas.1300772110

Focke, P.J., X. Wang, and H.P. Larsson. 2013. Neurotransmitter transporters: Structure meets function. *Structure.* 21:694–705. http://dx.doi.org/10.1016/j.str.2013.03.002

Focke, P.J., A.W. Annen, and F.I. Valiyaveetil. 2015. Engineering the glutamate transporter homologue GltPh using protein semisynthesis. *Biochemistry.* 54:1694–1702. http://dx.doi.org/10.1021/bi501477y

Groeneveld, M., and D.J. Slotboom. 2010. Na^+:Aspartate coupling stoichiometry in the glutamate transporter homologue Glt_{Ph}. *Biochemistry.* 49:3511–3513. http://dx.doi.org/10.1021/bi100430s

Hänelt, I., D. Wunnicke, E. Bordignon, H.-J. Steinhoff, and D.J. Slotboom. 2013. Conformational heterogeneity of the aspartate transporter Glt_{Ph}. *Nat. Struct. Mol. Biol.* 20:210–214. http://dx.doi.org/10.1038/nsmb.2471

Hill, A.V. 1910. Proceedings of The Physiological Society: January 22, 1910. The possible effects of the aggregation of the molecules of huemoglobin on its dissociation curves. *J. Physiol.* 40:i–iv. http://dx.doi.org/10.1113/jphysiol.1910.sp001386

Jensen, S., A. Guskov, S. Rempel, I. Hänelt, and D.J. Slotboom. 2013. Crystal structure of a substrate-free aspartate transporter. *Nat. Struct. Mol. Biol.* 20:1224–1226. http://dx.doi.org/10.1038/nsmb.2663

Koshland, D.E., Jr., G. Némethy, and D. Filmer. 1966. Comparison of experimental binding data and theoretical models in proteins containing subunits. *Biochemistry.* 5:365–385. http://dx.doi.org/10.1021/bi00865a047

Kuriyan, J., B. Konforti, and D. Wemmer. 2012. The Molecules of Life: Physical and Chemical Principles. Garland Science, New York. 1032 pp.

Lolkema, J.S., H. Enequist, and M.E. van der Rest. 1994. Transport of citrate catalyzed by the sodium-dependent citrate carrier of *Klebsiella pneumoniae* is obligatorily coupled to the transport of two sodium ions. *Eur. J. Biochem.* 220:469–475. http://dx.doi.org/10.1111/j.1432-1033.1994.tb18645.x

Machtens, J.-P., D. Kortzak, C. Lansche, A. Leinenweber, P. Kilian, B. Begemann, U. Zachariae, D. Ewers, B.L. de Groot, R. Briones, and C. Fahlke. 2015. Mechanisms of anion conduction by coupled glutamate transporters. *Cell.* 160:542–553. http://dx.doi.org/10.1016/j.cell.2014.12.035

Monod, J., J. Wyman, and J.P. Changeux. 1965. On the nature of allosteric transitions: A plausible model. *J. Mol. Biol.* 12:88–118. http://dx.doi.org/10.1016/S0022-2836(65)80285-6

Mulligan, C., and J.A. Mindell. 2013. Mechanism of transport modulation by an extracellular loop in an archaeal excitatory amino acid transporter (EAAT) homolog. *J. Biol. Chem.* 288:35266–35276. http://dx.doi.org/10.1074/jbc.M113.508408

Perutz, M.F. 1989. Mechanisms of cooperativity and allosteric regulation in proteins. *Q. Rev. Biophys.* 22:139–237. http://dx.doi.org/10.1017/S0033583500003826

Reyes, N., C. Ginter, and O. Boudker. 2009. Transport mechanism of a bacterial homologue of glutamate transporters. *Nature.* 462:880–885. http://dx.doi.org/10.1038/nature08616

Reyes, N., S. Oh, and O. Boudker. 2013. Binding thermodynamics of a glutamate transporter homolog. *Nat. Struct. Mol. Biol.* 20:634–640. http://dx.doi.org/10.1038/nsmb.2548

Ryan, R.M., and J.A. Mindell. 2007. The uncoupled chloride conductance of a bacterial glutamate transporter homolog. *Nat. Struct. Mol. Biol.* 14:365–371. http://dx.doi.org/10.1038/nsmb1230

Ryan, R.M., E.L.R. Compton, and J.A. Mindell. 2009. Functional characterization of a Na^+-dependent aspartate transporter from *Pyrococcus horikoshii*. *J. Biol. Chem.* 284:17540–17548. http://dx.doi.org/10.1074/jbc.M109.005926

Sigworth, F.J. 1994. Voltage gating of ion channels. *Q. Rev. Biophys.* 27:1–40. http://dx.doi.org/10.1017/S0033583500002894

Slotboom, D.J., W.N. Konings, and J.S. Lolkema. 1999. Structural features of the glutamate transporter family. *Microbiol. Mol. Biol. Rev.* 63:293–307.

Verdon, G., S. Oh, R.N. Serio, and O. Boudker. 2014. Coupled ion binding and structural transitions along the transport cycle of glutamate transporters. *eLife.* 3:e02283. http://dx.doi.org/10.7554/eLife.02283

Weiss, J.N. 1997. The Hill equation revisited: uses and misuses. *FASEB J.* 11:835–841.

Wyman, J., and S.J. Gill. 1990. Binding and Linkage: Functional Chemistry of Biological Macromolecules. University Science Books, South Orange, NJ. 330 pp.

Yernool, D., O. Boudker, Y. Jin, and E. Gouaux. 2004. Structure of a glutamate transporter homologue from *Pyrococcus horikoshii*. *Nature.* 431:811–818. http://dx.doi.org/10.1038/nature03018

Yifrach, O. 2004. Hill coefficient for estimating the magnitude of cooperativity in gating transitions of voltage-dependent ion channels. *Biophys. J.* 87:822–830. http://dx.doi.org/10.1529/biophysj.104.040410

Zagotta, W.N., T. Hoshi, and R.W. Aldrich. 1994. Shaker potassium channel gating. III: Evaluation of kinetic models for activation. *J. Gen. Physiol.* 103:321–362. http://dx.doi.org/10.1085/jgp.103.2.321